An improved method for determining carrier densities via drive level capacitance profiling

Charles W. Warren,[1] Ellis T. Roe,[1] D. Westley Miller,[1] William N. Shafarman,[2] and Mark C. Lonergan[3,a)]
[1]*Department of Physics, University of Oregon, Eugene, Oregon 97403, USA*
[2]*Institute of Energy Conversion, University of Delaware, Newark, Delaware 19176, USA*
[3]*Department of Chemistry and Biochemistry, University of Oregon, Eugene, Oregon 97403, USA*

(Received 31 January 2017; accepted 29 April 2017; published online 15 May 2017)

We demonstrate that an analytic relationship between coefficients in the Taylor expansion of the junction capacitance can be exploited to yield more precise determinations of carrier densities in drive level capacitance profiling (DLCP). Improvements are demonstrated on data generated according to the DLCP theory and in measurements performed on a $CuIn_xGa_{1-x}Se_2$ device. We argue that the improved DLCP method is especially important for non-uniform devices, which are more susceptible to noise in the capacitance data used in DLCP because they require that the amplitude of the drive level be restricted. Importantly, the analysis does not require the collection of any data other than what is typically collected during a DLCP measurement while employing *fewer* independent parameters than the model that is typically used in DLCP. Thus, we expect that it will be readily adoptable by those who perform DLCP measurements. *Published by AIP Publishing.*
[http://dx.doi.org/10.1063/1.4983367]

Drive-level capacitance profiling (DLCP) was initially developed by Michelson *et al.* as a method to accurately determine charge density profiles in amorphous silicon films that contained high densities of deep gap states.[1] In materials with significant densities of interface states or deep defects, such as the polycrystalline thin films used in solar cells, conventional capacitance-voltage (C-V) profiling can lead to incorrect determinations of carrier densities and spatial profiles.[2,3] The principal reason for this is that C-V assumes that all charge response to the AC probe voltage occurs at the depletion edge.[4] DLCP analysis explicitly rejects this assumption, thus accounting for how the charge response is affected by defect states in the depletion region. As a result, DLCP should not overestimate the charge density due to the presence of deep defects or interface states—an assertion that has been confirmed by simulations.[2] However, DLCP is still susceptible to many of the same artifacts as C-V when applied to non-ideal device structures. Indeed, some have argued that it does not provide additional information relative to C-V.[5,6] This debate is beyond the scope of this work. Regardless, the use of DLCP has become common within the thin-film solar cell community including the application in the study of, e.g., $CuIn_xGa_{1-x}Se_2$ (CIGS),[2,7–9] CZTS,[10–14] and CdTe.[15,16] In the interest of aiding these communities, this letter demonstrates a straightforward method to determine drive-level carrier densities (N_{DL}) with more precision than the standard practice. This modified approach is easily implemented as it does not require the collection of any additional data beyond what is normally collected during a DLCP measurement.

The DLCP method exploits the dependence of junction capacitance on the magnitude of the AC probe voltage used to measure it. As described in detail by Heath *et al.*,[2] the junction capacitance (C) can be expressed as a function of the peak-to-peak value of the AC probe voltage (δV) applied at a frequency ω such that

$$C \equiv \frac{\delta Q}{\delta V} = \frac{A(\epsilon F_e + \rho_e x_e)}{\delta V}\left[\sqrt{1 + \frac{2\epsilon\rho_e \delta V}{(\epsilon F_e + \rho_e x_e)^2}} - 1\right]. \quad (1)$$

Here, δQ is the change in charge, A is the area of the device, and ϵ is the dielectric constant, while $\rho_e = |\rho(x_e)|$ and $F_e = |F(x_e)|$ are the magnitudes of the net charge density and the electric field at x_e. The quantity x_e is the location where δQ is generated and is defined to be the position at which the relevant band edge is exactly $E_e = k_B T \ln\left[2\pi\nu_0 T^2/\omega\right]$ from the Fermi energy E_F. As usual, k_B is the Boltzmann constant, T is the absolute temperature, and ν_0 is the thermal emission prefactor. Note that δV is defined to be positive despite the fact that it strictly applies a reverse bias to the junction.

It is advantageous to express Eq. (1) as a Taylor series in powers of δV

$$C = \sum_{n=0}^{\infty} C_n \delta V^n, \quad (2)$$

where

$$C_n = \binom{\frac{1}{2}}{n+1} \frac{A(2\epsilon\rho_e)^{n+1}}{(\epsilon F_e + \rho_e x_e)^{2n+1}}, \quad (3)$$

with the generalized binomial coefficient in Eq. (3) defined such that

$$\binom{m}{k} \equiv \frac{m(m-1)\ldots(m-k+1)}{k!}. \quad (4)$$

a)Electronic mail: lonergan@uoregon.edu

Note that the coefficients defined in this way can be negative (with $m = \frac{1}{2}$ and $k = 1$, 2, 3, and 4 the coefficients defined in Eq. (4) are: $\frac{1}{2}, -\frac{1}{8}, \frac{1}{16}$, and $-\frac{5}{128}$).

A standard DLCP measurement is carried out by measuring C as a function of δV and determining the coefficients C_0, C_1, and C_2 by fitting the data with a quadratic model with three independent parameters (i.e., $C = C_0 + C_1\delta V + C_2\delta V^2$ with C_0, C_1, and C_2 independent). The carrier density N_{DL} can then be calculated from the coefficients to give

$$N_{DL} = \frac{\rho_e}{q} = -\frac{C_0^3}{2q\epsilon A^2 C_1}. \tag{5}$$

However, note that Eq. (3) allows the higher order coefficients to be related to preceding coefficients in the series by the relation

$$C_{n+2} = \frac{(n+2)(2n+3)}{(n+3)(2n+1)}\frac{C_{n+1}^2}{C_n}. \tag{6}$$

A consequence of this is that every C_n with $n \geq 2$ is completely determined by C_1 and C_0 alone, e.g.,

$$C_2 = 2\frac{C_1^2}{C_0}, \tag{7}$$

and

$$C_3 = 5\frac{C_1^3}{C_0^2}. \tag{8}$$

Thus, upon treating C_2 as an independent parameter, the standard DLCP fitting model described above ignores these constraints. Indeed, a close inspection of Eq. (1) reveals that C vs. δV behavior has *exactly* two free parameters. Therefore, it is not surprising that the Taylor expansion also has exactly two free parameters.

In this letter, we will introduce alternative fitting models that explicitly enforce Eqs. (7) and (8) and examine how the choice of model impacts the DLCP measurement. The analysis of these models utilizes both analytically generated raw data and experiments on a CIGS solar cell. Capacitance measurements were carried out using a Stanford Research Systems (SRS) SR850 lock-in amplifier in conjunction with a SRS SR570 current-to-voltage preamplifier. In all cases, a lock-in frequency of 10 kHz was used. Sample temperature was controlled using a Linkam LTS350 stage in conjunction with a Linkam TP94 temperature controller and a Linkam LNP94 liquid nitrogen pump. For all measurements, the stage temperature was held at 200 K. The peak-to-peak magnitude of the AC probe voltage used for DLCP was varied from 30 mV to 90 mV. Note that the upper limit of this range is lower than values used in other studies.[1,2] This is necessary for devices in which $\rho(x)$ is nonuniform (as is the case here) due to a fundamental assumption of the DLCP method which requires that $\rho(x)$ is constant over a width $\delta x = C\delta V/A\rho(x)$.[2] For the purpose of obtaining an estimate of the maximum value of δV allowed by this assumption, we consider $\rho(x)$ to be approximately constant over δx if it varies by no more than 10% (i.e., the change in $\rho(x)$ over δx is required to be an order of magnitude smaller than $\rho(x)$ itself). For a typical graded CIGS device, $\rho(x)/q$ can vary by as much as $10^{16}\,\mathrm{cm}^{-3}\,\mu\mathrm{m}^{-1}$ with $\rho/q \approx 3 \times 10^{15}\,\mathrm{cm}^{-3}$.[17] Thus, having $\rho(x)$ varying by no more than 10% over δx requires δx be less than $\sim$0.03 μm. The condition $C \approx 20\ \mathrm{nF/cm^2}$ requires δV be less than $\sim$100 mV ($\sim$40 $\mathrm{mV_{rms}}$).

The properties of the CIGS device used in this work are summarized in Table I. The CIGS was deposited by a three-stage co-evaporation process, which results in films with the through-film composition and bandgap gradients.[18] The composition measured by x-ray fluorescence gave Cu/(In + Ga) = 0.88 and Ga/(In + Ga) = 0.26. The device structure is glass/Mo/CIGS/CdS/ZnO/ITO/grid.

This letter will examine three models used to fit C vs. δV data collected during a DLCP measurement:

- Model 1: $C = C_0 + C_1\delta V + C_2\delta V^2$. This is the model that is typically used when fitting DLCP data. The three coefficients C_0, C_1, and C_2 are assumed to be *independent*.
- Model 2: $C = C_0 + C_1\delta V + 2C_1^2\delta V^2/C_0$. This is simply Model 1 with Eq. (7) explicitly enforced, resulting in only two independent coefficients.
- Model 3: $C = C_0 + C_1\delta V + 2C_1^2\delta V^2/C_0 + 5C_1^3\delta V^3/C_0^2$. This is Model 2 with the addition of a third-order term that explicitly enforces Eq. (8). Note that this model still has only two independent coefficients.

Note that the linear model $C = C_0 + C_1\delta V$ will not be considered because it introduces large errors for C vs. δV data with a significant curvature. Such a curvature is commonly observed.[1,2] It is also possible to fit C vs. δV data with the functional form of Eq. (1) using a non-linear fitting routine. However, doing so results in negligible improvements in accuracy and precision compared to Model 3 (see Figures S1 and S2 in the supplementary material). Furthermore, the Taylor expansion form is more useful in the context of this work because it is more readily interpreted in terms of C vs. δV data (i.e., C_1 is the slope when $\delta V = 0$ and C_0 is the limit of the capacitance as $\delta V \to 0$). Given this, we will limit our discussion to the Taylor expansion forms.

Model 1 yields reasonable results if the C vs. δV data have a relatively high signal to noise ratio (SNR). However, because it ignores Eq. (7), it does not account for the fact that the curvature (C_2) is exactly determined by the slope at $\delta V = 0$ (C_1) and the capacitance intercept (C_0). For data with a sufficiently low SNR, this distinction is important because a second-order polynomial fit assuming three independent parameters might, e.g., incorrectly determine the sign and magnitude of C_2 due to random noise. Thus, Model 1 tends to overfit data and produces false curvature values. A C vs. δV data set (calculated from Eq. (1) with zero-mean Gaussian noise superposed) shown in Figure 1 illustrates how treating C_2 as an independent parameter can lead to inaccuracies in C_0 and C_1. In this case, Model 1 finds that $C_2 < 0$ (violating Eq. (3)), and thus, it underestimates both

TABLE I. Efficiency, fill factor, open-circuit voltage, and short-circuit current of the CIGS device studied.

Eff. (%)	FF (%)	V_{OC} (mV)	J_{SC} mA/cm^2)
13.7	73.0	609	30.9

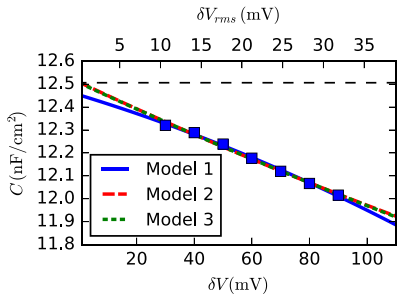

FIG. 1. Example of the C vs. δV data generated to create the histograms in Figure 2. Lines indicate the results of three fitting methods: Model 1, the standard second-order polynomial fit with three independent parameters (blue solid line); Model 2, a second-order polynomial fit with two independent parameters that enforces Eq. (7) (red dashed line); and Model 3, a third-order polynomial fit with two independent parameters that enforces Eqs. (7) and (8) (green dotted line). The correct value of the constant term C_0 is indicated by the horizontal dashed line. The error in C_0 is less than 0.5% for Model 1. However, Model 1 underestimates the magnitude of C_1 by over 30%.

C_0 and $|C_1|$. While the relative error in C_0 is generally negligible, the relative error in $|C_1|$ is often large enough to cause significant error in N_{DL}. Obviously, the fitting methods that explicitly enforce Eq. (7) (Models 2 and 3) are not susceptible to such errors.

Figure 2 shows a histogram of the error in N_{DL} relative to the correct carrier density, N_0. N_{DL} values were generated by fitting analytically generated C vs. δV data with each of the three models. The 5×10^4 analytic C vs. δV data sets were created by evaluating Eq. (1) with $\rho_e = qN_0$ and superposing zero-mean Gaussian noise. A relative standard deviation of $\sigma = 5 \times 10^{-4}$ was used, consistent with noise levels

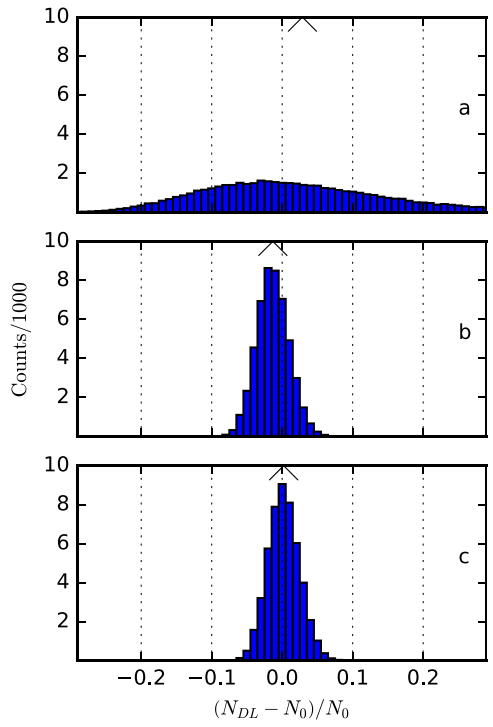

FIG. 2. Histogram of the relative error of N_{DL} with respect to the correct carrier density N_0 for (a) Model 1, a standard second-order polynomial fit with three independent parameters; (b) Model 2, a second-order polynomial fit with two independent parameters that explicitly enforces Eq. (7); and (c) Model 3, a third-order polynomial fit with two independent parameters that explicitly enforces Eqs. (7) and (8). Chevrons indicate the mean relative error.

observed in real measurements. In all cases, seven capacitance data points were used for the fits. Increasing the number of data points did not strongly affect the accuracy or precision of N_{DL} (see Figure S3 in the supplementary material). Figures 2(a), 2(b), and 2(c) show histograms of N_{DL} values calculated from Models 1, 2 and 3, respectively. As is clear from comparison of the histograms, Models 2 and 3 greatly improve the precision of N_{DL} relative to Model 1. Notice that fitting the data with Model 2 tends to slightly underestimate the value of N_{DL} and that the third-order term in Model 3 corrects this. Considering that the third-order term can be included in the fitting procedure without introducing any additional independent parameters, it is clearly beneficial to do so. Including higher order terms would be easy as well but doing so does not significantly improve the accuracy or precision of the fit.

An illustration of how effectively each model determines N_{DL} for varying degrees of noise in the capacitance data is shown in Figure 3. The relative standard deviation of N_{DL} (σ_{DL}) is plotted as a function of the relative standard deviation of the capacitance data, σ_C. The relative standard deviation σ_C was controlled via the random Gaussian noise that was superposed on the analytic capacitance values. As is clear in Figure 3, the relative standard deviation of N_{DL} is ~5 times smaller when using Model 2 or Model 3 as compared to Model 1. Considering that the systematic underestimation of N_{DL} by Model 2 is not captured in σ_{DL}, it is clear that the Model 3 is the preferred model.

An example of how different fitting models affect experimental DLCP data for a CIGS device is shown in Figure 4. The purpose of demonstrating our method experimentally is to show its improved precision. It should be emphasized that we make no claims regarding the accuracy of the data. This, however, is unimportant for the purposes of demonstrating improved precision. The data were collected using δV ranging from 10.6 to 31.8 mV_{rms} (30 to 90 mV peak-to-peak). This was not extended to 5 mV_{rms} (the smallest available AC probe voltage for many lock-in amplifiers and LCR meters) because the relative noise level at this AC amplitude resulted in data that did not appreciably improve the fits. Note that the N_{DL} values produced by each model were calculated from the same underlying C vs. δV data set. At larger reverse bias, where the C vs. δV data are relatively flat, noise has a large effect on the Model 1 fit and considerable error is

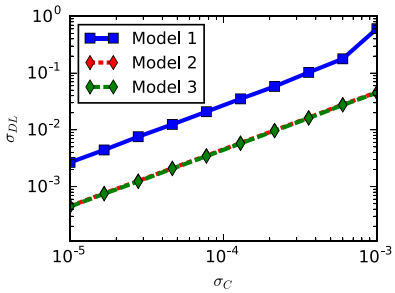

FIG. 3. The relative standard deviation of N_{DL}, σ_{DL}, as a function of the relative standard deviation of the capacitance data, σ_C. N_{DL} values were calculated from 5×10^4 analytic C vs. δV data sets with zero-mean Gaussian noise superposed with a relative standard deviation σ_C. Seven data points were used for the fits as illustrated in Figure 1.

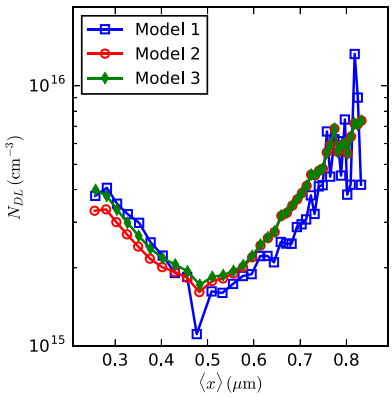

FIG. 4. Example of how fitting models affect drive-level profiles of a non-uniform CIGS device. Each profile is calculated from the same C vs. δV data set. Model 1 (blue squares) exhibits increased error for data taken at a larger reverse bias, where noise has a larger impact because the C vs. δV curve is relatively flat. Model 2 (red circles) alleviates this by enforcing Eq. (7) but slightly underestimates N_{DL} in forward bias where the third-order term is more important. Model 3 (green diamonds) includes the third-order correction.

introduced. Models 2 and 3 alleviate this issue by constraining C_2, but Model 2 is predicted to slightly underestimate N_{DL} in forward bias where the third-order term in Eq. (2) becomes more important (Figure 2). Model 3 includes the third-order term and is the most precise throughout the entire range of the profile. Note that these improvements can also be leveraged to increase the parameter space available to DLCP. An illustration of how the range of frequencies available to DLCP can be improved is shown in Figure S4 in the supplementary material. Examples of the underlying C vs. δV data sets used to produce N_{DL} values of Figure 4 are shown in Figure S5 in the supplementary material.

It is worth noting that the proposed improvement is primarily an increase in the precision of data provided by the DLCP measurement. Device properties such as non-ohmic back contacts are well known to induce artifacts in many capacitance based techniques, including DLCP, admittance spectroscopy, and C-V.[19,20] As in any such situation, systematic errors are necessarily introduced by violation of the underlying assumptions of the measurement. We emphasize that our method cannot intrinsically solve this problem. However, it could be used to better characterize non-ideal devices as it allows for higher precision even under noisy conditions such as at large DC biases and at extreme frequencies. If data under such conditions contain systematic errors, increased precision will inevitably be useful to correctly identify such anomalies. For instance, if a device is afflicted by a non-ohmic back contact, one could minimize its effect on DLCP data by measuring capacitance at low frequency.[19] However, capacitance measurements at low frequency can be noisy (see Figure S4 in the supplementary material), and thus, the improved precision offered by our method could be advantageous.

To summarize, we have demonstrated that the relationship between coefficients in the Taylor expansion of the junction capacitance can be exploited to yield more accurate fits of the C vs. δV data used in DLCP. This results in derived carrier densities, N_{DL}, that are more precise by a factor of 5 relative to those extracted using the standard method (Model 1). This is especially important for non-uniform devices, which are more susceptible to noise in C vs. δV data because they require that the range of δV be restricted. It is also important in devices that exhibit low SNR capacitance data. The experimentalist also has the option of trading increased precision for faster measurements if the capacitance SNR is high. As such, this method enables faster acquisition of DLCP data, particularly at low frequency. Based on a combination of real and simulated DLCP measurements, we have demonstrated that fitting C vs. δV data with a model that is accurate to third-order in δV (Model 3) realizes the aforementioned improvements in precision (or speed). Including terms higher than third-order did not result in meaningful improvements. Because the third-order model does not require collection of any additional data and has fewer independent parameters than the standard method, the improvements can be realized without significant cost to the experimentalist.

See supplementary material for theoretical and experimental comparisons of the full non-linear model [Eq. (1)] and Model 3, plots expanding on the effects of the noise in the data, and a demonstration of how Model 3 improves the precision of DLCP data at extreme frequencies relative to Model 1.

Device fabrication was carried out at IEC. Characterization, simulation, and theory work (performed at UO) were supported by the Department of Energy via the Bay Area Photovoltaic Consortium (Award No. DE-EE0004946).

[1]C. E. Michelson, A. V. Gelatos, and J. D. Cohen, Appl. Phys. Lett. **47**, 412 (1985).
[2]J. T. Heath, J. D. Cohen, and W. N. Shafarman, J. Appl. Phys. **95**, 1000 (2004).
[3]C. R. Crowell and G. I. Roberts, J. Appl. Phys. **40**, 3726 (1969).
[4]S. M. Sze, *Semiconductors Devices, Physics and Technology*, 2nd ed. (Wiley, New York, USA, 1985).
[5]M. Ćwil, M. Igalson, P. Zabierowski, C. A. Kaufmann, and A. Neisser, Thin Solid Films **515**, 6229 (2007).
[6]M. Cwil, M. Igalson, P. Zabierowski, and S. Siebentritt, J. Appl. Phys. **103**, 063701 (2008).
[7]J. Lee, J. D. Cohen, and W. N. Shafarman, Thin Solid Films **480–481**, 336 (2005).
[8]R. Caballero, C. Kaufmann, T. Eisenbarth, M. Cancela, R. Hesse, T. Unold, A. Eicke, R. Klenk, and H. Schock, Thin Solid Films **517**, 2187 (2009).
[9]P. T. Erslev, W. N. Shafarman, and J. D. Cohen, Appl. Phys. Lett. **98**, 062105 (2011).
[10]O. Gunawan, T. Gokmen, C. W. Warren, J. D. Cohen, T. K. Todorov, D. A. R. Barkhouse, S. Bag, J. Tang, B. Shin, and D. B. Mitzi, Appl. Phys. Lett. **100**, 253905 (2012).
[11]G. Brammertz, M. Buffiere, Y. Mevel, Y. Ren, A. E. Zaghi, N. Lenaers, Y. Mols, C. Koeble, J. Vleugels, M. Meuris, and J. Poortmans, Appl. Phys. Lett. **102**, 013902 (2013).
[12]H.-S. Duan, W. Yang, B. Bob, C.-J. Hsu, B. Lei, and Y. Yang, Adv. Funct. Mater. **23**, 1466 (2013).
[13]C.-J. Hsu, H.-S. Duan, W. Yang, H. Zhou, and Y. Yang, Adv. Energy Mater. **4**, 1301287 (2014).
[14]Y. S. Lee, T. Gershon, O. Gunawan, T. K. Todorov, T. Gokmen, Y. Virgus, and S. Guha, Adv. Energy Mater. **5**, 1401372 (2015).
[15]S. Demtsu, D. Albin, J. Sites, W. Metzger, and A. Duda, Thin Solid Films **516**, 2251 (2008).
[16]J. Boucher, D. Miller, C. Warren, J. Cohen, B. McCandless, J. Heath, M. Lonergan, and S. Boettcher, Sol. Energy Mater. Sol. Cells **129**, 57 (2014).
[17]K. Kim, H. Park, G. M. Hanket, W. K. Kim, and W. N. Shafarman, Prog. Photovoltaics **23**, 765 (2015).
[18]L. Chen, J. Lee, and W. N. Shafarman, IEEE J. Photovoltaics **4**, 447 (2014).
[19]T. Eisenbarth, T. Unold, R. Caballero, C. A. Kaufmann, and H.-W. Schock, J. Appl. Phys. **107**, 034509 (2010).
[20]J. V. Li, A. F. Halverson, O. V. Sulima, S. Bansal, J. M. Burst, T. M. Barnes, T. A. Gessert, and D. H. Levi, Sol. Energy Mater. Sol. Cells **100**, 126 (2012).